

Femtosecond two-dimensional spectroscopy from anharmonic vibrational modes of molecules in the condensed phase

K. Okumura and Y. Tanimura

Division of Theoretical Studies, Institute for Molecular Science, Myodaiji, Okazaki, Aichi 444, Japan

(Received 5 July 1996; accepted 5 May 1997)

We have developed a theory of the fifth-order off-resonant spectroscopy to study the effect of anharmonicity of molecular vibrational modes. The anharmonicity, as well as nonlinear dependence of polarizability on nuclear coordinates, can be the origin of the fifth-order Raman signal. A profile of the signal varies depending on the relative importance of the two effects—the anharmonicity and the nonlinearity. The anharmonicity of a potential can be distinguished from the other effects such as the nonlinearity or the inhomogeneity of vibrational modes. In order to carry out calculations analytically, we employ the multimode Brownian oscillator model and treat anharmonicity as perturbation to the harmonic vibrational modes. A simple analytical expression for the fifth-order polarization is obtained through a diagrammatic technique, called Feynman rule on the unified time path. Physical pictures for the analytical expression are given for a single mode system through numerical calculations and through double-sided Feynman diagrams. Applications to CHCl_3 and CS_2 are made where the third-order experiments are used to extract parameters. In the CS_2 case, the theoretical fifth-order signals are compared with recent experiment, which suggests some sign of anharmonicity. © 1997 American Institute of Physics. [S0021-9606(97)00331-0]

I. INTRODUCTION

The feature of inter- and intramolecular vibrational modes and their dephasing in liquids plays a central role in virtually all chemical processes in solution. The recent advent of ultrafast laser technology makes it possible to perform nonlinear vibrational experiments that can probe the information. Experiments conducted so far, including impulsive stimulated light scattering (ISS),¹ femtosecond optical Kerr effect (OKE),²⁻⁴ and far infrared (IR) absorption,⁵ have yielded spectral densities in the low-frequency range, providing characteristic properties of intermolecular nuclear degrees of freedom, both local and collective.

Recently, two-dimensional off-resonant spectroscopy was proposed to separate the inhomogeneous distribution of slowly varying parameters (e.g., due to local liquid configurations) from the total spectral distribution of nuclear time scale.⁶ This experiment uses two pairs of excitation pulses and related to the fifth-order nonlinearity. Experimental⁷⁻⁹ and theoretical¹⁰⁻¹³ studies have been made to explore possibility to detect such inhomogeneity. In this paper, we present another possibility of the fifth-order off-resonant experiments: detection of anharmonicity of vibrational modes with the help of the third-order experiments such as ISS or OKE.

The primary microscopic basis for understanding spectroscopic experiments can be normal modes analysis by molecular dynamics simulations.¹⁴⁻¹⁷ In this simulation method, calculation of the higher-order optical signals is demanding and the method to include quantum effects are not well established.¹⁷ On the other hand, if we employ the multimode Brownian oscillator model,^{18,19} analytical calculation can be performed quantum mechanically, though microscopic origins of the Brownian modes are sometimes obscured. In the Brownian model, collections of normal mode

oscillations can be interpreted as being represented by several primary (harmonic) modes coupled to the baths.

For the moment, we consider a system with a single Brownian coordinate Q to present experimental observables in terms of response functions. In the third-order off-resonant experiments, such as ISS and OKE, the signal is related to the two-time correlation function of the nuclear polarizability, $R^{(3)}(t) \sim \langle [\alpha(t), \alpha(0)] \rangle$, where $\alpha(t)$ is the polarizability in the Heisenberg representation [defined in Eq. (2.5)]. In such polarizability sensitive measurements, coordinate dependence of α is essential, since, if α is a c -number, $\alpha(t)$ commutes with $\alpha(0)$ and $R^{(3)}$ vanishes. If one expands polarizability in terms of the coordinate in the Heisenberg representation $Q(t)$, i.e., $\alpha(t) = \alpha_0 + \alpha_1 Q(t) + \alpha_2 Q^2(t)/2 + \dots$ (assuming $|\alpha_n Q^n| \gg |\alpha_{n+1} Q^{n+1}|$), then characters of $R^{(3)}$ are determined by $\alpha_1^2 \langle [Q(t), Q] \rangle$.

In the fifth-order off-resonant measurements, the signal is related to the three-time correlation function, $R^{(5)}(t, t') \sim \langle [[\alpha(t), \alpha(t')], \alpha(0)] \rangle$, which is defined in Eq. (2.6). Since the α_1^3 term (i.e., $\langle [[Q(t), Q(t')], Q] \rangle$) vanishes in the harmonic Brownian model, features of the signal can be captured by the term proportional to $\alpha_1^2 \alpha_2$ (i.e., $\langle [[Q^2(t), Q(t')], Q] \rangle$, etc.).

The easy-to-handle harmonic models in general are a fairly good but idealized model. The multimode (harmonic) Brownian model has been successfully used to study vibrational spectroscopy in liquids.¹⁹ From a molecular dynamics study, however, anharmonicities in the low frequency vibrational normal modes were found in water¹⁵ as well as in CS_2 .¹⁶ To reflect such anharmonicities, we include anharmonicity, expressed by $g_3 Q^3 + g_4 Q^4 + \dots$, into the primary Brownian mode. (More dynamics-oriented interpretation of anharmonicities is given in Sec. VI.) Although anharmonicities of each normal mode and of the Brownian modes are not

the same, we believe that the present study must be a good starting point to take the normal-mode anharmonicities into account.

In the present study we assume that the anharmonicity is weak so that it can be dealt with as perturbation. In addition, we assume that the polarizability is well approximated by first few terms in the expansion in terms of the primary coordinate Q . These assumptions may be reasonable to give representative results, although there may be a case where this standpoint is not appropriate.²⁰

Taking the anharmonicity into account, we re-examine the response function $R^{(3)}$ and $R^{(5)}$ presented above. Even in the anharmonic case, behavior of $R^{(3)}$ can still be described by $\alpha_1^2 \langle [Q(t), Q] \rangle$ as in the harmonic case, if the anharmonicity is not considerably strong.

In contrast, the main contribution to $R^{(5)}$ in the anharmonic case can be different from that in the harmonic case. For example, if the anharmonicity g_3 is significantly large compared with the nonlinear polarizability α_2 , the principal part can be the term proportional to $\alpha_1^3 g_3$ (i.e., $\langle [Q(t), Q(t'), Q] \rangle$).²¹ On the contrary, in the harmonic case, the dominant part is always the $\alpha_1^2 \alpha_2$ term as mentioned before. Since the time dependence of the $\alpha_1^3 g_3$ term is different from that of the $\alpha_1^2 \alpha_2$ term, $R^{(5)}$ can be used to detect anharmonicity. In realistic cases, depending on the relative ratio $\tilde{\alpha}_1^3 g_3 / (\tilde{\alpha}_1^2 \tilde{\alpha}_2)$ (where \tilde{x} denotes dimensionless quantity of x), the behavior of $R^{(5)}$ may vary since the time dependences of the terms proportional to $g_3 \alpha_1^3$ and to $\alpha_1^2 \alpha_2$ are different from each other.

Thus it is possible that anharmonicity and nonlinear coupling produce identical third-order signals, but rather different fifth-order signals. To demonstrate this, we calculated the fifth-order response function in the presence of anharmonicity of vibrational modes. To carry out calculations we employed the Feynman rule on the unified time path,^{22–25} which is suitable for the oscillators in the coordinate representation.²⁶ We obtained simple analytical expressions for the fifth-order off-resonant signal. In a single mode case, numerical calculations, as well as interpretations in terms of double-sided diagrams, were given to explain physical dynamics in the fifth-order processes. In the multimode cases, we calculated the fifth-order signal numerically by using parameters obtained from the third-order experimental data of CHCl_3 and CS_2 . By comparison of the numerical results with the recent fifth-order experimental data by Tokmakoff and Fleming,⁹ we found some sign of anharmonicity in CS_2 . We analyze the physical nature of the Brownian modes of CS_2 in Sec. VI.

II. THE THIRD- AND FIFTH-ORDER OFF-RESONANT EXPERIMENT

We consider a molecular system in the condensed phase irradiated with electronically off-resonant pulses. The off-resonant pulses allow us to selectively probe the vibrational dynamics associated with the electronic ground state through

the polarizability. The effective Hamiltonian for a system irradiated with the off-resonant electric field $E(\mathbf{r}, t)$ is given by^{18,19}

$$H_{\text{eff}} = H_g(P, Q) - E^2(\mathbf{r}, t) \alpha_Q, \quad (2.1)$$

where $H_g(P, Q)$ is a molecular vibrational Hamiltonian on an electronic ground-state potential surface and α_Q is the coordinate dependent polarizability. Here, P and Q collectively represent the momenta and coordinates of the vibrational motions.

If the system is described by a single nuclear mode specified by its coordinate Q and momentum P (generalization to a multimode nuclear system is dealt with in Sec. V), the polarizability and the vibrational Hamiltonian are, respectively, expressed as

$$\alpha_Q = \alpha_0 + \alpha_1 Q + \frac{\alpha_2}{2} Q^2 + \dots, \quad (2.2)$$

$$H_g(P, Q) = \frac{P^2}{2M} + \frac{M\Omega^2}{2} Q^2 + V(Q) + \sum_{i=1}^N \left[\frac{p_i^2}{2m_i} + \frac{m_i \omega_i^2}{2} \left(q_i - \frac{c_i Q}{m_i \omega_i^2} \right)^2 \right]. \quad (2.3)$$

Here, $V(Q)$ is the anharmonicity of the potential

$$V(Q) = \frac{g_3}{3!} Q^3 + \frac{g_4}{4!} Q^4 + \dots, \quad (2.4)$$

and c_i is the coupling constant between the system (Q) and the bath (q_i).

This Hamiltonian $H_g(P, Q)$ can describe a dissipative system in the condensed phase, since the Euler–Lagrange equation for $Q(t)$ in this system has the friction term

$$M \int dt' \gamma(t-t') \dot{Q}(t'),$$

where $\gamma(t)$ is specified by the bath parameters (m_i, ω_i, c_i) and is proportional to c_i^2 . (We have to set $N \rightarrow \infty$ to describe the dissipation.) We can parameterize our theory in terms of $\gamma(t)$ instead of specifying all the values (m_i, ω_i, c_i). In the following we employ the Ohmic dissipation model $\gamma(t) = \gamma \delta(t)$, where γ is a constant. [This choice of $\gamma(t)$ is possible only after we let $N \rightarrow \infty$.] The strength of dissipation is reflected in the constant γ .

The physical observables in optical experiments can be related to the response functions $R^{(n)}$,¹⁹ which are expectation values of multicommutators. The response function related to the third- and fifth-order off-resonant experiment are defined by

$$R^{(3)}(\tau_1) = \frac{i}{\hbar} \langle [\alpha(\tau_1), \alpha(0)] \rangle, \quad (2.5)$$

$$R^{(5)}(\tau_1, \tau_2) = \left(\frac{i}{\hbar} \right)^2 \langle [[\alpha(\tau_1 + \tau_2), \alpha(\tau_1)], \alpha(0)] \rangle, \quad (2.6)$$

where $[\dots]$ is the commutator ($[A, B] \equiv AB - BA$), $\langle \dots \rangle$ ($= \text{Tr}[\rho_g \dots]$) is the expectation by the initial distribution at the inverse temperature β

$$\rho_g = e^{-\beta H_g(P, Q)} / \text{Tr}[e^{-\beta H_g(P, Q)}], \quad (2.7)$$

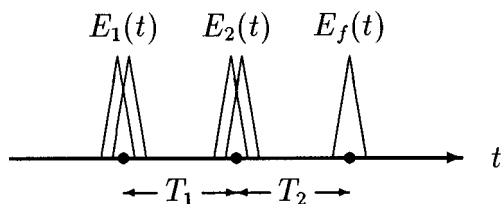


FIG. 1. Pulse configuration for the fifth-order experiment. The two pairs of pulses are applied to the system, which are followed by the last probe pulse. The temporal profiles of the pulses $E_1(t)$, $E_2(t)$, and $E_f(t)$ peak at $t = -T_1 - T_2$, $t = -T_2$, and $t = 0$, respectively.

and $\alpha(t)$ is the Heisenberg operator associated with the electronic ground state Hamiltonian

$$\alpha(t) = e^{(i/\hbar)H_g(P,Q)t} \alpha_Q e^{-(i/\hbar)H_g(P,Q)t}. \quad (2.8)$$

Now we explain pulse configuration for the third- and fifth-order experiment. In general, the electric field $E(\mathbf{r}, t)$ in the $(2n+1)$ th order experiment is given by $E(\mathbf{r}, t) = E_f(\mathbf{r}, t) + \sum_{j=1}^n E_j(\mathbf{r}, t)$, where $E_j(\mathbf{r}, t) = E_j(t)(e^{i\omega_j t - i\mathbf{k}_j \cdot \mathbf{r}} + e^{i\omega_j' t - i\mathbf{k}_j' \cdot \mathbf{r}}) + \text{c.c.}$ and $E_f(\mathbf{r}, t) = E_f(t)e^{i\omega_f t - i\mathbf{k}_f \cdot \mathbf{r}} + \text{c.c.}$ in which c.c. stands for the complex conjugate. For example, in the third-order experiment (ISS or OKE), the envelopes $E_1(t)$ and $E_f(t)$ peak at $t = -T_1$ and $t = 0$, respectively ($n = 1$). Thus, in the third order, we apply the system two simultaneous pulses (center frequencies ω_1, ω_1' and wave vectors $\mathbf{k}_1, \mathbf{k}_1'$) at $t = -T_1$ and then the probe pulse (ω_f and \mathbf{k}_f) at $t = 0$.

Pulse configuration for the fifth-order experiment is given by the above expression for $E(\mathbf{r}, t)$ with $n=2$ and is described in Fig. 1.^{6,19} The temporal profiles of the pulses $E_1(t)$, $E_2(t)$, and $E_f(t)$ peak at $t = -T_1 - T_2$, $t = -T_2$, and $t = 0$, respectively; the two pairs of pulses are applied to the system, which are followed by the last probe pulse. The first pair (ω_1, ω_1' and $\mathbf{k}_1, \mathbf{k}_1'$) is irradiated at the time $t = -T_1 - T_2$, the second (ω_2, ω_2' and $\mathbf{k}_2, \mathbf{k}_2'$) at $t = -T_2$, and the final pulse (ω_f and \mathbf{k}_f) at $t = 0$.

The polarizations relevant to the third-order and the fifth-order experiments are, respectively, given by^{6,19}

$$P^{(3)}(t) = [E_f(t)e^{i(\omega_f t - \mathbf{k}_f \cdot \mathbf{r})} + \text{c.c.}] \int_0^\infty d\tau_1 R^{(3)}(\tau_1) \times 2|E_1(t - \tau_1)|^2 [1 + \cos\{\Delta\omega_1(t - \tau_1) - \Delta\mathbf{k}_1 \cdot \mathbf{r}\}], \quad (2.9)$$

$$P^{(5)}(t) = [E_f(t)e^{i(\omega_f t - \mathbf{k}_f \cdot \mathbf{r})} + \text{c.c.}] \int_0^\infty d\tau_1 \int_0^\infty d\tau_2 \times R^{(5)}(\tau_1, \tau_2) 2|E_1(t - \tau_1 - \tau_2)|^2 \cdot 2|E_2(t - \tau_2)|^2 \times [1 + \cos\{\Delta\omega_1(t - \tau_1 - \tau_2) - \Delta\mathbf{k}_1 \cdot \mathbf{r}\}] \times [1 + \cos\{\Delta\omega_2(t - \tau_2) - \Delta\mathbf{k}_2 \cdot \mathbf{r}\}], \quad (2.10)$$

where we have introduced $\Delta\omega_n = \omega_n' - \omega_n$, and $\Delta\mathbf{k}_n = \mathbf{k}_n' - \mathbf{k}_n$.

For impulsive pump experiments, we set

$$E_f(t) = \delta(t),$$

$$E_1(t) = \delta(t + T_1),$$

$$E_2(t) = \delta(t + T_1 + T_2). \quad (2.11)$$

Then the signals, which are observed in a phase-matched direction^{1,2,7-9} and related to the square of the polarization, are given by (up to a proportionality constant)

$$I^{(3)} = |R^{(3)}(T_1)|^2, \quad (2.12)$$

$$I^{(5)} = |R^{(5)}(T_1, T_2)|^2. \quad (2.13)$$

III. FEYNMAN RULES FOR RESPONSE FUNCTIONS

In this section we derive the response functions of a single mode system by using the Feynman rule on the unified-time path (UTP). Originally the Feynman rule was developed to calculate the vacuum (the ground state) expectation values of operators in an anharmonic system.²⁷ A similar diagrammatic rule was initiated by using the Matsubara Green's functions (propagators) to obtain the thermal expectation.²⁷ The Feynman rule on UTP is an extension of these rules to obtain the nonequilibrium expectation values, or the real-time correlation functions.

The common feature of these three methods is that expectation values are given by the sum of Feynman diagrams. Each Feynman diagram consists of points connected by lines and corresponds to an analytical expression by the rule in a unique way.

We define here some terms for diagrammatic expansions; examples are given shortly. The i -point in a diagram is a point from which i lines go out. Any i -point is either an external point or an internal point; the former originates from an operator for which the expectation value is calculated, while the latter from anharmonicity. The internal point is also called vertex and the line is called propagator. The internal i -point is also called i -vertex.

To illustrate the Feynman rule, we first consider the diagrammatic expansion of $R^{(3)}$. According to the expansion of the polarizability, $R^{(3)}$ can be expressed as

$$R^{(3)}(T_1) = \frac{i}{\hbar} \alpha_1^2 \langle [Q(T_1), Q(0)] \rangle + \frac{i}{\hbar} \alpha_1 \alpha_2 \langle [Q^2(T_1), Q(0)] + [Q(T_1), Q^2(0)] \rangle + \frac{i}{\hbar} \alpha_2^2 \langle [Q^2(T_1), Q^2(0)] \rangle + \dots, \quad (3.1)$$

where $Q(t)$ is the Heisenberg operator

$$Q(t) = e^{(i/\hbar)H_g(P,Q)t} Q e^{-(i/\hbar)H_g(P,Q)t}. \quad (3.2)$$

The diagrammatic expansion of the first term is given by

$$\frac{i}{\hbar} \alpha_1^2 \langle [Q(T_1), Q(0)] \rangle = \text{---} \circ \text{---} + \text{---} \circ \text{---} + \text{---} \circ \text{---} \text{---} \circ \text{---} + \text{---} \circ \text{---} \text{---} \circ \text{---} + \text{---} \circ \text{---} \text{---} \circ \text{---} + \text{---} \circ \text{---} \text{---} \circ \text{---} + \dots, \quad (3.3)$$

where we consider the g_3 and g_4 anharmonicities explicitly and draw diagrams up to the second order in these anharmonicities.

In each of the above diagrams the two white circles are external 1-points and correspond to the operators $\alpha_1 Q(T_1)$ and $\alpha_1 Q(0)$. The black circles are vertices or internal points. For example, the second diagram have a 4-vertex or an internal 4-point from which four lines go out; this vertex corresponds to the anharmonic interaction $g_4 Q^4$.

From these diagrams, we know the dependences of the diagrams on the parameters α_i and g_i ; the number and types of circles determine them. The first diagram is proportional to α_1^2 , the second to $\alpha_1^2 g_4$, the third to $\alpha_1^2 g_3^2$ and so forth.

These diagrams can be generated as follows. First, we determine an operator for which the expectation is calculated, which fixes the external points that have to be used in diagrams. In the above case, the external points to be used are the two 1-points represented by white circles, which correspond to the operators $\alpha_1 Q(T_1)$ and $\alpha_1 Q(0)$. Second, we determine which order of the expectation we calculate, which fixes the internal points. In the case of the order of g_3^2 [the third and the fourth diagrams in Eq. (3.3)], the internal points are two 3-points represented by black circles.

Third, we make all possible connected diagrams out of the given external and internal points by jointing them with lines (propagators). In the g_3^2 case, we can make two different diagrams [the third and fourth in Eq. (3.3)] from two 1-points and two 3-points. In the course, we can use as many lines as we need and all possible diagrams have to be taken into account in the calculation of that order.

The term proportional to $\alpha_1^2 g_3$ vanishes in Eq. (3.3). Diagrammatically this simply means that we cannot make connected diagrams out of two 1-points and one 3-point. In general, we can easily pick up nonzero contributions by these diagrammatic rules.

In the Feynman rule for the vacuum expectation value and for the thermal expectation, analytical expressions for each diagram would be obtained from the above diagrams. However, in the rule on the unified-time path (UTP) for the nonequilibrium expectation, we add indices, “+,” “-,” or “3,” to all the extremities of the lines in order to derive analytical expressions. These diagrams with indices are called *specified diagrams*, while the diagrams as given above are called *simplified diagrams* in the UTP rule.²⁴ The specified diagrams corresponding to Eq. (3.3) are given by

$$\frac{i}{\hbar} \alpha_1^2 \langle [Q(T_1), Q(0)] \rangle = \text{---} \circ \text{---} + \text{---} \circ \text{---} + \text{---} \circ \text{---} \text{---} \circ \text{---} + \text{---} \circ \text{---} \text{---} \circ \text{---} + \text{---} \circ \text{---} \text{---} \circ \text{---} + \text{---} \circ \text{---} \text{---} \circ \text{---} + \dots, \quad (3.4)$$

R^{AH} and R^{NL} . In other words, we can use the fifth-order experiment to determine the relative importance of anharmonicity and nonlinearity.

The effectiveness of this strategy depends on how the two main contributions, R^{AH} and R^{NL} , behave differently for

various parameters. Before checking this point numerically, we explain that the two contributions come from very different physical processes.

To have a physical insight, we employ the double-sided Feynman diagrams.¹⁹ For the third-order experiment we have

$$R^{(3)}(T_1) = \begin{array}{c} \begin{array}{cccc} 0 & 1 & 0 & \\ \bullet & \bullet & & \\ \hline 0 & 0 & 0 & \\ \leftarrow T_1 \end{array} + \begin{array}{cccc} 0 & 1 & 1 & \\ \bullet & & & \\ \hline 0 & 0 & \bullet & 1 \\ \leftarrow T_1 \end{array} + \begin{array}{cccc} 0 & 0 & 0 & \\ & & & \\ \hline 0 & \bullet & \bullet & 0 \\ \leftarrow T_1 \end{array} + \begin{array}{cccc} 0 & 0 & 1 & \\ & & & \\ \hline 0 & \bullet & & 1 \\ \leftarrow T_1 \end{array} + \dots \end{array} \quad (4.1)$$

Here, the first four diagrams correspond to the first term in Eq. (3.9) or the diagram in Eq. (3.5).

In these diagrams, the lower horizontal line corresponds to the time evolution (from the left to the right) of the bra and the upper line to that of the ket. Black circles stand for the laser interaction. If the polarizability is linear, the laser interaction changes the vibrational state of the system $|v\rangle$ into the state $|v \pm 1\rangle$. This is because we assume the linear polarizability $\alpha_1 Q$, in which Q can be expressed as $a + a^\dagger$. Here, a and a^\dagger are the annihilation and creation operators ($a^\dagger|v\rangle = |v+1\rangle$, etc.). For simplicity, we have assumed that the system is initially in the ground state $|0\rangle$ in Eq. (4.1).

The first diagram can be interpreted as follows. At first a system is in the population state $|0\rangle\langle 0|$. At $t = -T_1$ the ket $|0\rangle$ interacts with the laser, and the system is in the coherence state $|1\rangle\langle 0|$ in the next period T_1 . Here, the coherence state

refers to the state $|i\rangle\langle j|$ ($i \neq j$), and the population state to $|i\rangle\langle i|$. At $t=0$ the ket again interacts with the laser, and the system is brought back to the state $|0\rangle\langle 0|$. (The final state of the bra and ket have to be the same state so that the case where the final state becomes $|2\rangle\langle 0|$ should be excluded.) Thus during the T_1 period the system in the state $|1\rangle\langle 0|$ undergoes the coherence relaxation.

Similarly, we find that in the second diagram the system is in the state $|1\rangle\langle 0|$ in the T_1 period, whereas in the third and fourth diagrams it is in the state $|0\rangle\langle 1|$ in the T_1 period. (In general, the two diagrams different only in the positions of the rightmost interaction make the same contribution.) Thus the third-order experiment probes the dynamics of the coherence state $|0\rangle\langle 1|$ or $|1\rangle\langle 0|$ (the dephasing process) for the period T_1 .

The diagrams of R^{AH} in Eq. (3.13) are given by

$$R^{AH}(T_1, T_2) = \begin{array}{c} \begin{array}{cccccc} 0 & 1 & 0 & \times & 1 & 0 \\ \bullet & \bullet & & & & \\ \hline 0 & 0 & 0 & 0 & 0 & 0 \\ \leftarrow T_1 \quad \leftarrow T_2 \end{array} + \begin{array}{cccccc} 0 & 0 & 1 & \times & 0 & 1 \\ & & & & & \\ \hline 0 & \bullet & 1 & 1 & 1 & 1 \\ \leftarrow T_1 \quad \leftarrow T_2 \end{array} + \dots \end{array} \quad (4.2)$$

In above diagrams the cross stands for the anharmonic interaction $g_3 Q^3$, which changes the state $|v\rangle$ into the state $|v \pm 1\rangle$ (aaa^\dagger , etc.) or $|v \pm 3\rangle$ ($a^\dagger a^\dagger a^\dagger$, etc.). The cross can be placed on either upper or lower T_2 portion of the horizontal lines; this can be seen from the fact that the integration $\int_0^\infty dt$ in Eq. (3.13) reduces to the one over the T_2 period $\int_{T_1}^{T_1+T_2} dt$ (due to the step function contained in $D^{(-+)}$).

All the diagrams which have to be considered for the first term in Eq. (3.13) are obtained by the first diagram in Eq. (4.2) by moving black circles and the cross to the lower line. For example, the second diagram is obtained by moving the leftmost circle to the lower line. Thus, we have 2^4 diagrams in total.

In the first diagram, the system is in the coherence state

$|1\rangle\langle 0|$ in the T_1 period, while it changes the state during the T_2 period in two ways: $|0\rangle\langle 0| \rightarrow |1\rangle\langle 0|$ and $|2\rangle\langle 0| \rightarrow |1\rangle\langle 0|$.

By studying all the diagrams, we find that in the T_1 period the system is in the coherence state while in the T_2

period it changes the state from a population state to a coherence state, or from a coherence state to another coherence state.

The diagrams of R^{NL} are given by

$$R^{NL}(T_1, T_2) = \begin{array}{c} \begin{array}{cccc} 0 & 1 & 0 & 0 \\ \bullet & \bullet & \circ & \bullet \\ \hline 0 & 0 & 0 & 0 \\ \leftarrow T_1 \quad \leftarrow T_2 \end{array} \\ + \begin{array}{cccc} 0 & 0 & 0 & 1 \\ \bullet & \bullet & \bullet & \bullet \\ \hline 0 & 1 & 1 & 1 \\ \leftarrow T_1 \quad \leftarrow T_2 \end{array} \\ + \dots \end{array} \quad (4.3)$$

In these diagrams, the white circle stands for the laser interaction through the nonlinear polarizability $\alpha_2 Q^2$. This interaction changes the state $|v\rangle$ into $|v \pm 2\rangle$ ($a^\dagger a^\dagger$, etc.) or does not change the state (aa^\dagger , etc.).

The diagrams are classified into two types for R^{NL} : In one type, only the rightmost circle is white [corresponding to the first diagram in Eq. (3.12)] and, in the other, only the middle circle is white [corresponding to the second in Eq. (3.12)]. Each type has 2^3 diagrams in the harmonic case.

By studying all the 2×2^3 diagrams, we find that during the T_1 period the system is in a coherence state, while it keeps either the population state or the coherence state in the T_2 period.

Based on the above analysis, we expect that the T_1 dependences of $R^{(3)}$, R^{AH} , and R^{NL} may have similar property since in all cases the dynamics of the coherence state $|0\rangle\langle 1|$ and $|1\rangle\langle 0|$ is probed in the T_1 period. In addition, we expect that the T_2 dependences of R^{AH} and R^{NL} may look different. Note that, however, the present analysis based on double-sided diagram fails to include the effect of dissipation so that the argument may be reasonable only in weak damping cases.

In order to carry out numerical calculations, we rewrite the expressions of signals given in the previous section in dimensionless quantities. First, the dimensionless propagator $f(t)$ is defined by

$$f(t) = \frac{\Omega}{\zeta} e^{-\gamma t/2} \sin \zeta t. \quad (4.4)$$

Note here that the ‘‘frequency’’ ζ is being allowed to be complex to include over and underdamped motion. Then, the dimensionless third-order signal is given by, $\tilde{I}^{(3)}(T_1) \equiv |\tilde{R}^{(3)}(T_1)|^2$, where

$$\tilde{R}^{(3)}(T_1) \equiv \frac{\hbar}{\alpha_0^2} R^{(3)}(T_1) = \tilde{a}_1^2 f(T_1) + \dots \quad (4.5)$$

Here,

$$\tilde{a}_i = \frac{\alpha_i}{\alpha_0} \left(\frac{\hbar}{M\Omega} \right)^{i/2}. \quad (4.6)$$

The dimensionless spectral distribution is expressed as

$$\tilde{J}(\omega) \equiv \frac{\hbar \Omega_0}{\alpha_0^2} J(\omega) = \tilde{\Omega} \tilde{a}_1^2 \frac{\tilde{\omega} \tilde{\gamma}}{(\tilde{\omega}^2 - \tilde{\Omega}^2)^2 + \tilde{\omega}^2 \tilde{\gamma}^2} + \dots, \quad (4.7)$$

where

$$\tilde{\Omega} = \Omega/\Omega_0, \quad \tilde{\gamma} = \gamma/\Omega_0, \quad (4.8)$$

with Ω_0 being an arbitrary unit of frequency.

The correction terms represented by ‘‘...’’ in Eq. (4.7) were calculated in Ref. 23 in a different context. The results show that the correction terms approach to zero when (1) the anharmonic parameter becomes smaller, (2) the damping constant γ/Ω becomes larger, or (3) the mode frequency $\hbar\Omega\beta$ becomes larger (for a fixed temperature $1/\beta$). This means that, even for low frequency modes in liquids where $\hbar\Omega$ can be much less than $1/\beta$, the correction term can be negligible if the anharmonic parameter is small enough. In the following numerical calculations, we use several set of parameters. In all cases, including CHCl_3 and CS_2 cases below, we have checked that the correction terms given in Ref. 23 are small and negligible.

The largest contributions to $\tilde{R}^{AH} \equiv \hbar^2 R^{AH}/\alpha_0^3$ and $\tilde{R}^{NL} \equiv \hbar^2 R^{NL}/\alpha_0^3$ are given by

$$\tilde{R}^{AH}(T_1, T_2) = -\tilde{g}_3 \tilde{a}_1^3 \int_{T_1}^{T_1+T_2} \Omega dt f(T_1+T_2-t) \times f(t-T_1) f(t), \quad (4.9)$$

$$\tilde{R}^{NL}(T_1, T_2) = \tilde{a}_1^2 \tilde{a}_2 f(T_2) [f(T_1+T_2) + f(T_1)], \quad (4.10)$$

where

$$\tilde{g}_i = \frac{g_i}{\hbar\Omega} \left(\frac{\hbar}{M\Omega} \right)^{i/2}. \quad (4.11)$$

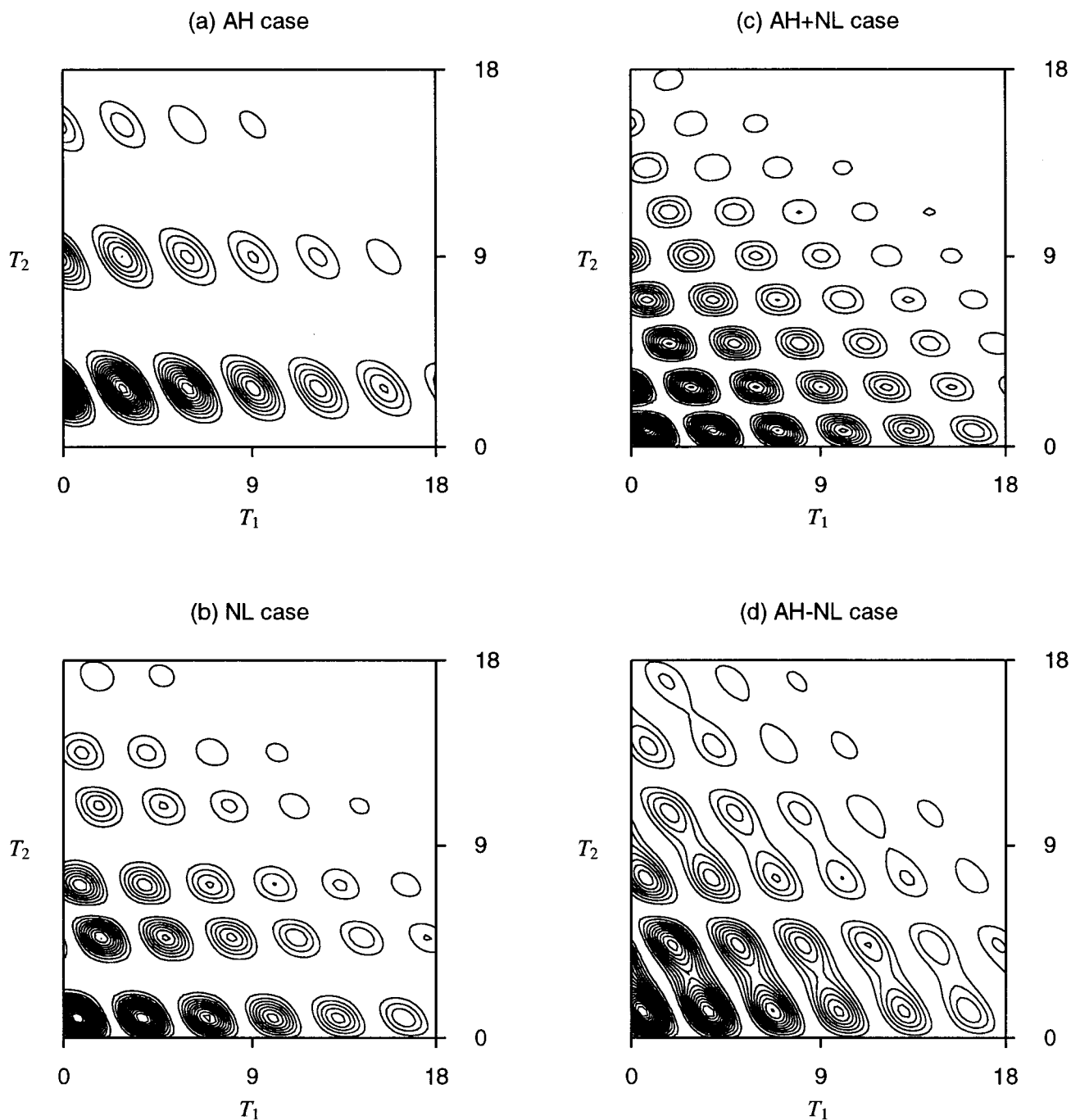


FIG. 3. The contour plots of the fifth-order signal from a weak damping mode with $\gamma/\Omega=0.1$. The parameters $(\bar{g}_3, \bar{\alpha}_2)$ are (0.01, 0), (0, 0.01), (0.01, 0.01), and $(-0.01, 0.01)$ in (a), (b), (c), and (d), respectively. The frequency Ω is normalized to unity.

Using these dimensionless expressions, we performed numerical calculations for the Ohmic damping. The fifth-order signals defined by $\tilde{I}^{(5)}(T_1, T_2) \equiv |\tilde{R}^{AH}(T_1, T_2) + \tilde{R}^{NL}(T_1, T_2)|^2$ are presented for a weak damping constant (Fig. 3) and for a strong damping constant (Fig. 4). The case where anharmonicity (g_3) is much stronger than nonlinearity (α_2) is discussed by (a) AH case; the opposite case is discussed by (b) NL case. The cases where anharmonicity and

nonlinearity are comparable are discussed by the two cases (c) and (d), which are different in the relative sign of g_3 and α_2 .

In the weak damping case (Fig. 3), the signals oscillate with the frequency 2Ω along T_1 in all the cases (a)–(d). This is the same oscillation as that of $R^{(3)}(T_1)$, as clearly seen from Eq. (3.9). This supports the conclusion drawn from the double-sided Feynman diagrams that the T_1 dependences of

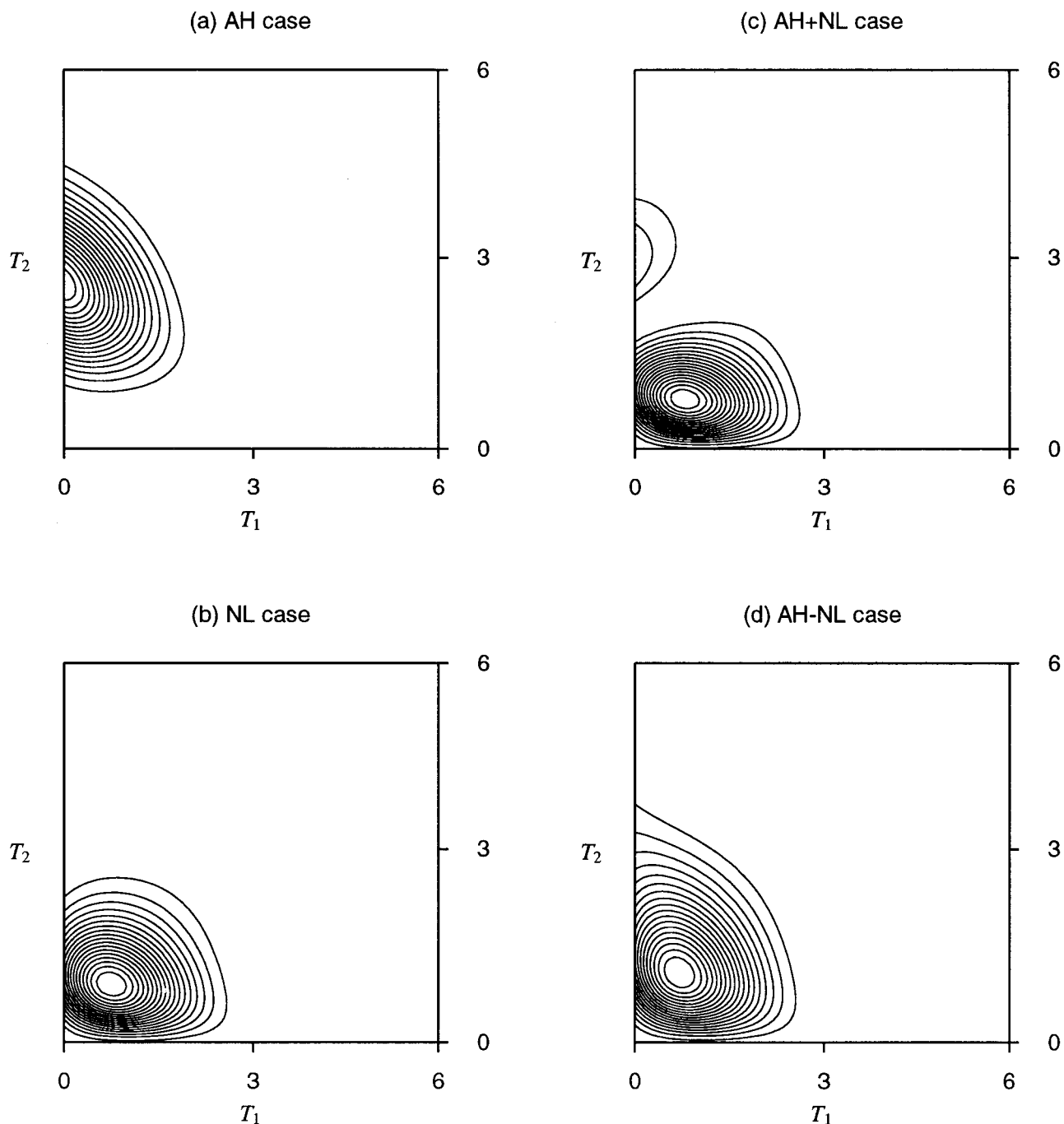


FIG. 4. The contour plots of the fifth-order signal from a strong damping mode with $\gamma/\Omega=1.0$. The other parameters are the same as in Fig. 3.

$R^{(3)}$, R^{AH} , and R^{NL} are similar at least for weak damping.

On the contrary, along T_2 , the signals in the case (a)–(d) look rather different. In the case (a)–(d), the signals along T_2 are superpositions of one, two, three, and three oscillation (s) of the frequency 2Ω , respectively. The way of interference among these components in case (c) is opposite to that in case (d) due to relative sign difference of g_3 and α_2 . This also supports the conclusion on the T_2 dependences of the signals drawn from the double-sided diagrams.

Under strong damping (Fig. 4), the signals in the cases

(a)–(d) show very different profile. In the AH case, the signal is distinctly asymmetric with respect to T_1 and T_2 axis, while it is fairly symmetric in the NL case. Another feature in the AH case is that the signal does not have initial rise along T_1 axis within a certain range of T_2 ; it only decays from a certain value along T_1 . On the other hand, the signal rises initially, reaches a peak, and then shows decay along both axis in the NL case. The signals in cases (c) and (d) can be understood as superpositions of those in cases (a) and (b).

In this way we have shown that two different system can

produce identical third-order signals but rather different fifth-order signals.

V. SIGNALS FROM MULTIMODE SYSTEMS

A generalization to the multimode system is straightforward. The multimode Hamiltonian is given by Eq. (2.1) with

$$H_g(P, Q) = \sum_s \left[\frac{P_s^2}{2M_s} + \frac{M_s \Omega_s^2}{2} Q_s^2 + V_s(Q_s) \right] + \sum_s \sum_{i=1}^N \left[\frac{P_{s,i}^2}{2m_{s,i}} + \frac{m_{s,i} \omega_{s,i}^2}{2} \left(q_{s,i} - \frac{c_{s,i}}{m_{s,i} \omega_{s,i}^2} Q_s \right)^2 \right]. \quad (5.1)$$

Here, Q_s and $V_s(Q_s)$ are the coordinate of the s th mode and the anharmonicity of the potential for the s th mode, respectively. As in the single mode case, we employ the Ohmic dissipation model and we parameterize the theory in terms of the damping constant γ_s instead of giving the values $(m_{s,i}, \omega_{s,i}, c_{s,i})$.

The anharmonicity V_s is given by

$$V_s(Q_s) = \hbar \Omega_s \left(\frac{\tilde{g}_{3s}}{3!} \tilde{Q}_s^3 + \frac{\tilde{g}_{4s}}{4!} \tilde{Q}_s^4 + \dots \right), \quad (5.2)$$

where the dimensionless coordinate \tilde{Q}_s is defined by $Q_s = \tilde{Q}_s \sqrt{\hbar / (M_s \Omega_s)}$.

In this Hamiltonian $H_g(P, Q)$, all the modes (specified by s) are assumed to be mutually independent. This assumption may be reasonable, particularly if the mode frequencies Ω_s are well separated in magnitude.

For the polarizability α_Q in Eq. (2.1), in addition to the linear model defined by $\alpha_Q = \alpha_0 (1 + \sum_s \tilde{a}_{1s} \tilde{Q}_s)$, we consider two simple models: *mode noncoupling model* and *mode coupling model*.

In the mode noncoupling (MNC) model, the polarizability is given by

$$\alpha_Q = \alpha_0 \sum_s \exp[\tilde{a}_{1s} \tilde{Q}_s] - \alpha_0 (N_s - 1), \quad (5.3)$$

where \tilde{a}_{1s} is a dimensionless expansion parameter, and N_s is the number of modes. The modes in this system can be treated as independent with each other and the total response function is given by the sum of the response function for each mode. The response functions are given in Appendix C.

In the mode coupling (MC) model, we assume^{6,19}

$$\alpha_Q = \alpha_0 \exp \left[\sum_s \tilde{a}_{1s} \tilde{Q}_s \right]. \quad (5.4)$$

The modes in this model are no longer independent and they interact with each other through radiation fields. However, we can calculate response functions rather easily even in this model, if we use the collective coordinate $\tilde{Q} \equiv \sum_s \tilde{a}_{1s} \tilde{Q}_s$ as a main variable in the calculation. For details and the expressions of the response functions in this model, see Appendix C.

Polarizability in both the MC and MNC models coincides with that in the linear model up to the linear term. (The

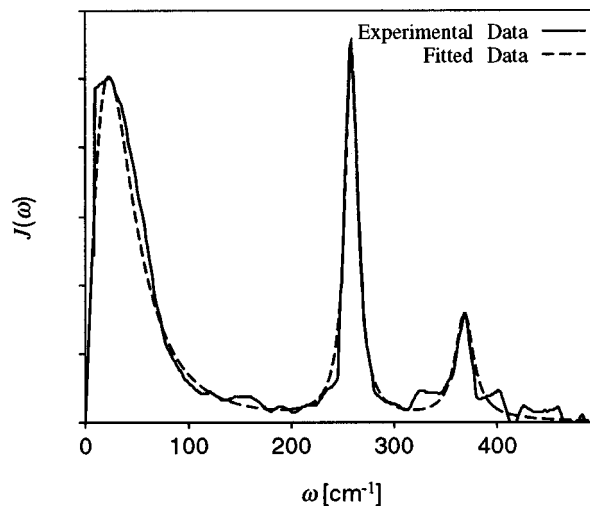


FIG. 5. The third-order signals for CHCl_3 . The experimental data in Ref. 3 (solid line) are well simulated by the three-mode model (broken line).

linear term $\alpha_0 \tilde{a}_{1s} \tilde{Q}_s$ shall be symbolically denoted α_1 in the following.) This is the reason two expressions of the third-order $R^{(3)}$ in Appendix C are the same within the approximation. The difference between polarizabilities in the two models appears in the square term (denoted α_2); the MC model has coupling terms such as $\tilde{Q}_1 \tilde{Q}_2$, while the MNC does not. This is the reason the fifth-order signals in the two models are different from each other (see Appendix C).

The fifth-order expressions for the multimode system can be classified into two parts as in the single mode case: one originating from nonlinearity and the other from anharmonicity. The former nonlinear contribution in the MC model, called R^{NLMC} , is different from that in the MNC model, called R^{NL} . The latter anharmonic contributions in the two models are the same and are called R^{AH} .

The third-order expression involves the independent parameters Ω_s , γ_s , and \tilde{a}_{1s} (see Appendix C). R^{AH} involves the parameter \tilde{g}_{3s} in addition to the third-order parameters Ω_s , γ_s , and \tilde{a}_{1s} . On the other hand, R^{NL} and R^{NLMC} are specified only by the third-order parameters. This is because, in the MC and MNC models, the coefficient of the second nonlinearity is determined by \tilde{a}_{1s} . Thus from the third-order experiment, we can determine the parameters Ω_s , γ_s , and \tilde{a}_{1s} , but we cannot determine the remaining parameters \tilde{g}_{3s} . The remaining parameters \tilde{g}_{3s} should be determined through the fifth-order experiment.

To demonstrate the results in the multimode case, we calculate the fifth-order signals for chloroform (CHCl_3) and for carbon disulfide (CS_2) by using parameters obtained from third-order experiments. Validity of various assumptions of the current theory will be discussed in the next section.

The third-order experiment of CHCl_3 ³ can be well explained by the multimode Hamiltonian with three modes as shown in Fig. 5, where the parameters (in the unit $[\text{cm}^{-1}]$) are given by

$$\eta_1 = 1.17 \quad \Omega_1 = 39.00 \quad \gamma_1 = 77.0$$

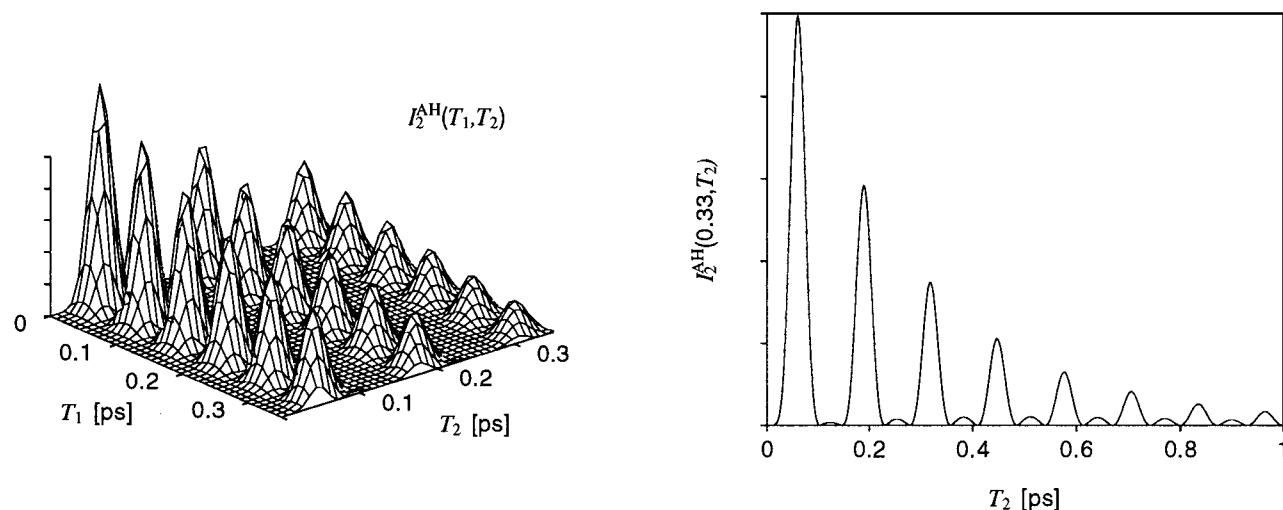


FIG. 6. The fifth-order signal of CHCl_3 for the AH2 case. The graph in the right is the signal at $T_1=0.33[\text{ps}^{-1}]$.

$$\eta_2=2.10 \quad \Omega_2=258.5 \quad \gamma_2=15.0 \quad (5.5)$$

$$\eta_3=1.25 \quad \Omega_3=368.5 \quad \gamma_3=22.0.$$

Here, we have introduced the strength of the mode

$$\eta_s = \Omega_s \tilde{a}_{1s}^2. \quad (5.6)$$

By using the above set of parameters, we calculate and compare the fifth-order signal of CHCl_3 in two considerably simple cases. In one case (AH2 case), we assume that only the second mode Ω_2 has anharmonicity ($\tilde{g}_{31} = \tilde{g}_{33} = 0, \tilde{g}_{32} \neq 0$) and that the polarizability is linear [$\alpha_Q = \alpha_0(1 + \sum_s \tilde{a}_{1s} Q_s)$]. Since the value of \tilde{g}_{32} determines only the absolute magnitude of the signal and does not contribute to profile of the signal, here we set it to unity. In the other case (NL case), we assume that all the modes are harmonic in the MNC model.

The fifth-order signal $I^{(5)}(T_1, T_2) = |R^{(5)}(T_1, T_2)|^2$ in the AH2 case is given in Fig. 6. The features of the signal are

similar to those in Fig. 3(a) since only the Ω_2 mode comes into play in this model; the two plots in Fig. 6 complement the contour plot in Fig. 3(a). Compared with the plots in Fig. 6, the plots in Fig. 7 are quite complicated due to interference of the three modes. The difference between the two cases are significant enough to be distinguished by experiments.

We next apply our result to carbon disulfide (CS_2), for which the fifth-order experiments have been done extensively.⁷⁻⁹ As shown in Ref. 7, the third-order experiments on CS_2 are well explained by the two-mode system specified by the parameters (in $[\text{cm}^{-1}]$)

$$\eta_L=1.00 \quad \Omega_L=12.9 \quad \gamma_L=43.0 \quad (5.7)$$

$$\eta_H=2.20 \quad \Omega_H=39.2 \quad \gamma_H=63.7.$$

We examined the mode noncoupling (MNC) and the mode coupling (MC) models, in addition to the linear model,

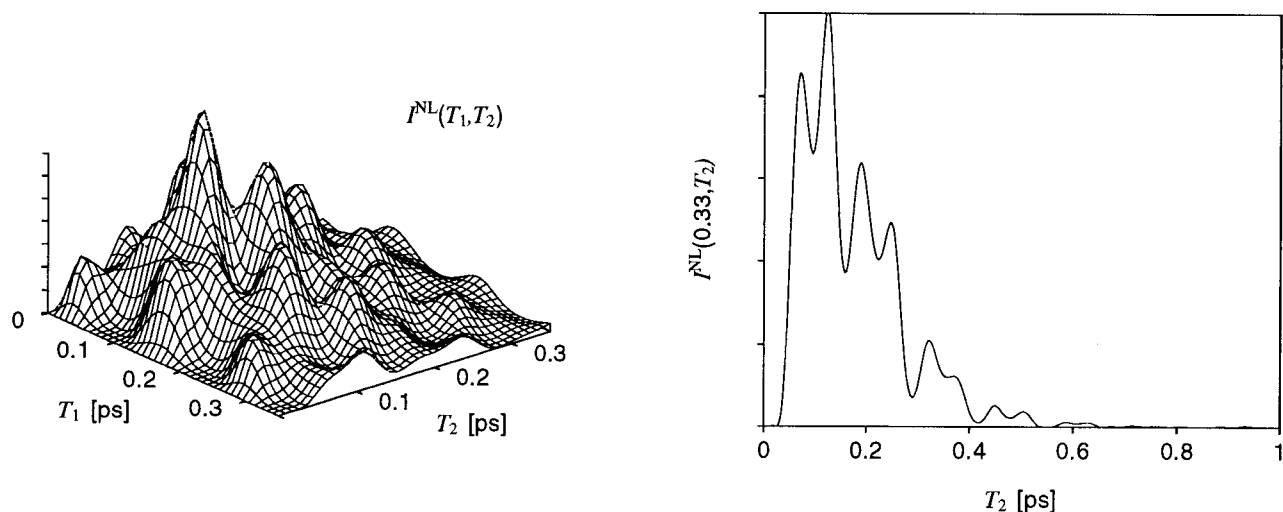


FIG. 7. The fifth-order signal of CHCl_3 for the NL case. The graph in the right is the signal at $T_1=0.33[\text{ps}^{-1}]$.

by using this set of parameters and by changing remaining free parameters \tilde{g}_{3L} and \tilde{g}_{3H} . After a careful examination, we found that the MC model is the best of the three. Within a rather broad range of anharmonicity $\tilde{g}_{3H}/\tilde{a}_{1H} = -6$ to 0 with $\tilde{g}_{3L} = 0$, the MC model gives fairly reasonable fits to the experimental result (Fig. 8).

All the signals in Fig. 8 resemble the experimental results (given in Fig. 10 of Ref. 9) in the following three points: (S1) the 2D signal decays asymmetrically in the two time variables T_1 and T_2 . (S2) along T_2 axis with fixed T_1 , the signal first rises from zero, reaches a peak and then decays with smaller time constant than that of the third-order signal. (S3) slowest decay rate along T_1 axis is almost identical to that of third-order signal.

However, there are following two differences between the experimental signal and the calculated signal in Fig. 8: (D1) the experimental signal has no inertial rise along the T_1 axis around $T_2 = 0 - 500$ [fs] (the signal at $T_1 = 0$ has a non-zero value), while the calculated signal rises from $T_1 = 0$ [fs] to the peak around $T_1 = 120$ [fs]. The ridge along T_2 axis (around $T_1 = 100 - 200$ [fs]) observed in the calculated signals is not seen in the experimental signal. (D2) in the experiment the slowest decay along the T_2 axis is about three times faster than that along the T_1 axis, while in the calculated cases the former is faster but not three times faster than the latter.

The main characters of the strongly damped anharmonic contribution to the signal is that it has nonzero value at $T_1 = 0$ and shows no inertial rise in a certain range of T_2 [see Fig. 4(a), for example] as has been observed in the experiments. We thus suspect that anharmonicity of the Ω_H mode plays some role in the fifth-order signal, although it is difficult to determine the qualitative ratio g_{3H}/a_{1H} as mentioned before. (Inclusion of the anharmonicity into the lower frequency mode Ω_L deteriorates the fits.)

As seen above, the theoretical signals cannot perfectly fit the experimental signal. Since the reasons for this have been already discussed in the literature,⁷⁻⁹ we do not iterate them here. It should be noticed that the difference between our analysis and previous ones is only inclusion of anharmonicity which is assumed to be rather weak in the above and thus can not be the fundamental reason for the discrepancy.

VI. DISCUSSION

In this section, we discuss validity of the assumptions of weak anharmonicity of the potential and of weak nonlinearity of the polarizability ($\alpha_1 \gg \alpha_2$) in real substances. For intramolecular modes these assumptions may be reasonable since the relevant value of \tilde{Q}_s is confined to a small region around an equilibrium configuration. For low frequency intermolecular modes, here we explain some more detail by taking the CS_2 case as an example.

Since the third order signal can be well fitted by the two modes Ω_L and Ω_H , the following simple physical picture has been employed in the literature (see, for example, Refs. 7 and 8): By the first pair of pulses, molecules are excited due to the strong (anisotropic) polarizability, and start to librate

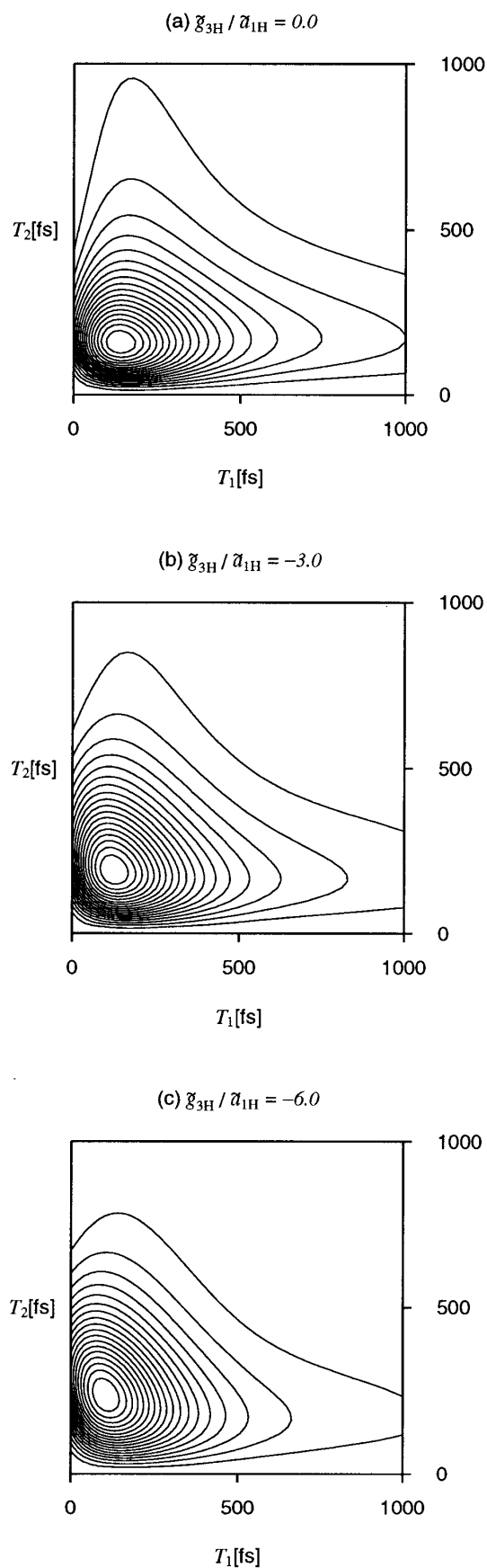


FIG. 8. The fifth-order signal of CS_2 for the mode coupling (MC) model at (a) $\tilde{g}_{3H}/\tilde{a}_{3H} = 0.0$, (b) $\tilde{g}_{3H}/\tilde{a}_{3H} = -3.0$, (c) $\tilde{g}_{3H}/\tilde{a}_{3H} = -6.0$. to be compared with Fig. 10 in Ref. 9.

in phase to the other excited molecules in the potential wells formed by surrounding molecules. This coherently excited motion decays by the loss of the phase relations among the excited molecules. After this decay, the initial isotropic polarizability can not be restored, because the molecules excited by the first pair of pulses have perturbed their environment, forming a net orientation. This anisotropic distribution of molecular orientation finally decays by diffusion. This bimodal process may be observed by the final probe pulse. From this point of view, the Ω_H mode has its origin in the coherently excited intermolecular librational motion and the Ω_L mode in the slowest bulk diffusive motion.

The fast librational motion may be influenced by the local environment and thus be inhomogeneous, while the diffusive dynamics may be caused by a random process and thus be homogeneous. Accordingly, Tominaga and Yoshihara as well as Tokmakoff and Fleming simulated the signal taking into the inhomogeneous effects for the higher frequency mode(s). However, it was found that the inhomogeneous effects are not so large in their analysis. This is the reason we employed homogeneous two modes here.

Thus it is natural that the librational motion be described by an anharmonic Brownian oscillator Ω_H . To justify the description of diffusive motion by Ω_L , it should be noted that in the Brownian oscillator model a vibrational mode is not necessarily a physical vibrational mode; in an overdamped case where $\Omega_s^2 < \gamma_s^2/4$, the third-order response function (in the harmonic case) can be expressed as a product of a rising function and a decaying function

$$\tilde{R}_s^{(3)}(t) = \tilde{a}_1^{-2} \frac{\Omega_s}{2\zeta'_s} (1 - e^{-t/\tau_{R_s}}) e^{-t/\tau_{D_s}}, \quad (6.1)$$

where $1/\tau_{R_s} = 2\zeta'_s \equiv 2\sqrt{\gamma_s^2/4 - \Omega_s^2}$ and $1/\tau_{D_s} = \gamma/2 - \zeta'_s$. This form with exponential rise constant τ_{R_s} and decay constant τ_{D_s} has been widely used in previous studies of the third-order experiment (see, for example, Ref. 4). In other words, the Brownian oscillator model is a convenient mathematical tool which can deal with a vibrational motion ($\Omega_s^2 > \gamma_s^2/4$) and a diffusive motion ($\Omega_s^2 < \gamma_s^2/4$) in a unified way.

As considered above, the anharmonic Brownian oscillator model seems to be a fairly reasonable modeling for low frequency modes in liquids. The assumption of weak nonlinearity of polarizability ($\alpha_1 \gg \alpha_2$) also fits the above interpretation, is a mathematically simple assumption that is easy to handle, and thus can be a reasonable starting point of the theory. Accordingly, the assumption of weak nonlinearity has been successfully and widely used for CS_2 in the literature.^{4,7-9}

In this study only the third-order anharmonicity (i.e., $g^3 Q^3$) surfaces and it makes the leading order contribution to the fifth-order off-resonance signal in the linear-polarization approximation. Though the fourth-order anharmonicity (i.e., $g^4 Q^4$) plays a minor role in the fifth-order experiments, it is possible to take into account such effects by a simple generalization of the present study. As shown in the separate article,²⁴ we can explore higher-order anharmonicity through higher-order experiments. For example, the effects of the

fourth-order anharmonicity can be larger than those of the third-order, in the seventh-order spectroscopy (related to the four-time correlation function $\langle [[\alpha(t_1), \alpha(t_2)], \alpha(t_3)], \alpha(t_4)] \rangle$).²⁴

The analysis in the present article was focused on off-resonant measurements using optical pulses. Equivalent experiments can be carried out by using infrared pulses to probe the vibrational transitions.²⁸ In such a case we should replace the interaction $E^2(\mathbf{r}, t)\alpha_Q$ in the effective Hamiltonian Eq. (2.1) by $E(\mathbf{r}, t)\mu_Q$. Here, μ_Q is the transition dipole moment. The present formulation can be adapted to this case by simply replacing the multitime correlation functions of $\alpha(t)$ by the corresponding correlation function of $\mu(t)$. The advantages of the infrared experiment is, for example, that lower order nonlinearity is required [the infrared photon echo (third-order) and the Raman echo (seventh-order) experiments both measure the three-time response function] although ultrafast technology of infrared laser is not developed well. Despite the formal similarity of the off-resonant optical and the resonant infrared experiments, the information is complementary since the correlation functions of α and μ carry different information as was shown in the water case.²⁹

VII. CONCLUSION

In this paper, we derived the fifth-order nuclear response function for the fifth-order off-resonant experiments. The anharmonicity of the vibrational modes was treated as perturbation. It is stressed here that the signal is sensitive to relative importance of the anharmonicity and the nonlinearity, since both effects can be observed as the largest contribution to the signal. On the other hand, the third-order signal is insensitive to neither anharmonicity nor nonlinear coordinate dependence of polarization, since the largest contribution depends on neither the anharmonicity nor the nonlinearity.

Based on analytical expressions, double-sided diagrams, and numerical calculations, we showed that anharmonicity and nonlinear coupling can produce identical third-order signals, but very different fifth-order signal, explicitly for a single mode system.

We also calculated the fifth-order two-dimensional signals for CHCl_3 and CS_2 using the spectral distribution observed in the third-order experiments such as ISS. We compared our results with experimental data on CS_2 obtained by Tokmakoff and Fleming, which indicates a sign of anharmonicity in CS_2 .

ACKNOWLEDGMENTS

The authors appreciate fruitful discussions with S. Mukamel, K. Tominaga, K. Yoshihara, and T. Tahara. They would also like to thank A. Tokmakoff, G. R. Fleming, T. Steffen, and K. Duppen for sending their preprints prior to publications. We greatly acknowledge the support from the Japanese Society for the Promotion of Science and Grand-in-Aid for Scientific Research from the Japan Ministry of Education, Science, Sports, and Culture.

APPENDIX A: RESPONSE FUNCTIONS AND THEIR GENERATING FUNCTIONAL

In this Appendix we introduce the generating function $W(J)$ and show that the response functions can be generated from $W(J)$ through derivative by J . Following arguments are the basis of the Feynman rule on the unified time path (UTP). The derivation of the rule itself is given in Ref. 24 which relies on the arguments here.

In order to calculate response functions, we consider the system given in Eq. (2.1) with artificial external sources at $E(\mathbf{r}, t) = 0$. The source is introduced for calculational convenience and shall be set to zero at the end. The time evolution operator and the initial density matrix in the presence of the artificial external field $J \equiv (J_1, J_2, J_3)$ are given by

$$K^{J_\alpha}(t_2, t_1) = T e^{-\frac{i}{\hbar} \int_{t_1}^{t_2} dt [H_g(P, Q) - J_\alpha(t) Q]} \quad (\alpha = 1, 2),$$

$$\rho^{J_3} = T e^{-\frac{1}{\hbar} \int_0^{\hbar\beta} dt [H_g(P, Q) - J_3(t) Q]}, \quad (\text{A1})$$

where T is the time-ordering operator, which reorders operators according to the time associated with the operators. The nonequilibrium generating functional $W(J)$ for the connected (or cumulant) response function is then defined by

$$e^{(i/\hbar)W(J)} = \text{Tr} [\rho^{J_3} [K^{J_2}(\infty, 0)]^\dagger K^{J_1}(\infty, 0)]. \quad (\text{A2})$$

Here, Tr means the trace over both the system (Q) and the bath (q_i) coordinates. The three operators, $K^{J_1}(\infty, 0)$, $[K^{J_2}(\infty, 0)]^\dagger$, and ρ^{J_3} , correspond to the real time evolution of the ket, that of the bra, and the imaginary time evolution for the initial state, respectively. These three time evolutions are, respectively, associated with the C_1 -, C_2 -, and C_3 -path in Fig. 2.

Introducing the time ordering operator T_C on the unified time path $C = C_1 + C_2 + C_3$, which reorders operators along the arrow shown in Fig. 2, we have

$$e^{(i/\hbar)W(J_C)} = \text{Tr} [T_C e^{-\frac{i}{\hbar} \int_C dt [H_g - J_C(t) Q]}, \quad (\text{A3})$$

where $J_C(t) = J_\alpha(t)$ if t is on C_α ($\alpha = 1, 2, 3$).

We employ simple notations for derivative operators

$$\partial_1(t) \equiv \frac{\hbar}{i} \frac{\partial}{\partial J_1(t)},$$

$$\partial_2(t) \equiv -\frac{\hbar}{i} \frac{\partial}{\partial J_2(t)}.$$

Note that we add the minus sign for ∂_2 in the above, but it should be removed if we replace $W(J)$ with $W(J_C)$ in the following expressions since $\delta_C(t_2, t'_2) = -\delta_C(t_2 - t'_2)$ [$t_2, t'_2 \in C_2$].

We can show

$$\begin{aligned} & \langle Q(t_2) Q(t_3) Q(t_1) \rangle_c \\ & \equiv \langle Q_2 Q_3 Q_1 \rangle - \langle Q_2 Q_3 \rangle \langle Q_1 \rangle - \langle Q_3 Q_1 \rangle \langle Q_2 \rangle \\ & \quad - \langle Q_2 Q_1 \rangle \langle Q_3 \rangle + 2 \langle Q_2 \rangle \langle Q_3 \rangle \langle Q_1 \rangle \\ & = \partial_1(t_1) \partial_2(t_2) \frac{1}{2} [\partial_1(t_3) + \partial_2(t_3)] \frac{i}{\hbar} W(J) \Big|_{J=0}, \quad (\text{A4}) \end{aligned}$$

for $t_3 > t_2 > t_1$, where $Q(t_i)$ is denoted by Q_i . In the above we have set $J = 0$ after performing the derivatives in order to recover the original system.

In general the expectation of the multicommutator is equal to the cumulant expectation. For example, we have

$$\langle [[Q_3, Q_2], Q_1] \rangle_c = \langle [[Q_3, Q_2], Q_1] \rangle, \quad (\text{A5})$$

and $R^{(5)}$ can be expressed as

$$R^{(5)}(T_1, T_2) = \left(\frac{i}{\hbar} \right)^2 \langle [[\alpha(T_1 + T_2), \alpha(T_1)], \alpha(0)] \rangle_c.$$

Note here the last subscript c is the difference from the previous definition of $R^{(5)}$.

Thus, from relations similar to Eq. (A4) and from the definition

$$\partial^{(+)}(t) \equiv \frac{\hbar}{i} \frac{\partial}{\partial J_1(t)} + \frac{\hbar}{i} \frac{\partial}{\partial J_2(t)},$$

$$\partial^{(-)}(t) \equiv \frac{1}{2} \left(\frac{\hbar}{i} \frac{\partial}{\partial J_1(t)} - \frac{\hbar}{i} \frac{\partial}{\partial J_2(t)} \right),$$

we have

$$\begin{aligned} R^{(5)}(T_1, T_2) & = \left(\frac{i}{\hbar} \right)^2 [\alpha_{\partial_1(0)} \alpha_{\partial_1(T_1)} - \alpha_{\partial_1(0)} \alpha_{\partial_2(T_1)} \\ & \quad - \alpha_{\partial_2(0)} \alpha_{\partial_1(T_1)} + \alpha_{\partial_2(0)} \alpha_{\partial_2(T_1)}] \\ & \quad \times \alpha_{\partial^{(-)}(T_1 + T_2)} \frac{i}{\hbar} W(J) \Big|_{J=0}, \quad (\text{A6}) \end{aligned}$$

where

$$\alpha_{\partial(t)} = \alpha_0 + \alpha_1 \partial(t) + \frac{1}{2} \alpha_2 [\partial(t)]^2 + \dots \quad (\text{A7})$$

In the same way we have the expression for the response functions $R^{(3)}$, R^{AH} , and R^{NL} in terms of $W(J)$

$$R^{(3)}(T_1) = \frac{i}{\hbar} \alpha_1^2 \partial^{(+)}(0) \partial^{(-)}(T_1) \frac{i}{\hbar} W(J) \Big|_{J=0}, \quad (\text{A8})$$

$$\begin{aligned} R^{AH}(T_1, T_2) & = \left(\frac{i}{\hbar} \right)^2 \alpha_1^3 \partial^{(+)}(0) \partial^{(+)}(T_1) \\ & \quad \times \partial^{(-)}(T_1 + T_2) \frac{i}{\hbar} W(J) \Big|_{J=0}, \quad (\text{A9}) \end{aligned}$$

$$\begin{aligned}
R^{NL}(T_1, T_2) &= \left(\frac{i}{\hbar}\right)^2 \alpha_1^2 \alpha_2 [\partial^{(+)}(0) \partial^{(+)}(T_1) \partial^{(-)}(T_1 + T_2) \\
&\quad + \partial^{(+)}(0) \partial^{(+)}(T_1) \partial^{(-)}(T_1) \\
&\quad + \partial^{(+)}(0) \partial^{(-)}(0) \partial^{(+)}(T_1)] \\
&\quad \times \partial^{(-)}(T_1 + T_2) \frac{i}{\hbar} W(J) \Big|_{J=0}. \quad (\text{A10})
\end{aligned}$$

The derivative operators appearing in Eqs. (A8)–(A10) correspond to external points in the specified diagrams. For example, two 1-points and one 2-point in the first diagram in Eq. (3.12) come from the derivative operator $\partial^{(+)}(0) \partial^{(+)}(T_1) \partial^{(-)}(T_1 + T_2) \partial^{(-)}(T_1 + T_2)$ in Eq. (A10).

APPENDIX B: ANALYTICAL EXPRESSION FOR $R^{AH}(T_1, T_2)$

To perform the integration over t in Eq. (3.13), we first use the formula

$$\begin{aligned}
&\sin x_1 \sin x_2 \sin x_3 \\
&= -\frac{1}{4} \sum_{\epsilon_2, \epsilon_3 = \pm 1} \epsilon_2 \epsilon_3 \sin(x_1 + \epsilon_2 x_2 + \epsilon_3 x_3). \quad (\text{B1})
\end{aligned}$$

The result of the integration is given by

$$R^{AH}(T_1, T_2) = -g_3 \alpha_1^3 [F(T_1) - F(T_1 + T_2)], \quad (\text{B2})$$

where

$$\begin{aligned}
F(t) &= \frac{1}{4(M\zeta)^3} \sum_{i=1}^4 (-1)^i \frac{e^{-\gamma(T_2+t)/2}}{\gamma^2/4 + (\zeta a_i)^2} \\
&\quad \times \left\{ \frac{\gamma}{2} \sin[\zeta(a_i t + b_i)] + \zeta a_i \cos[\zeta(a_i t + b_i)] \right\}. \quad (\text{B3})
\end{aligned}$$

Here, $(a_1, a_2, a_3, a_4) = (1, -1, -3, -1)$ and $(b_1, b_2, b_3, b_4) = (T_2, T_2, 2T_1 + T_2, 2T_1 + T_2)$.

APPENDIX C: RESPONSE FUNCTIONS FOR MULTIMODE SYSTEMS

In this Appendix, we give expressions for response functions for the multimode Hamiltonian. The largest contributions to $R^{(3)}(T_1)$ and to the counterparts of R^{AH} and R^{NL} (introduced in the single mode case) are presented below under the assumption $\tilde{a}_{1s} \ll 1$.

In the mode noncoupling (MNC) model, the response functions are given by the sum of the response functions for each modes as mentioned before

$$R^{(3)}(T_1) = \sum_s \frac{\alpha_0^2}{\hbar} \tilde{a}_{1s}^2 f_s(T_1), \quad (\text{C1})$$

$$R^{(5)}(T_1, T_2) = R^{AH}(T_1, T_2) + R^{NL}(T_1, T_2), \quad (\text{C2})$$

where

$$\begin{aligned}
R^{AH}(T_1, T_2) &= -\frac{\alpha_0^3}{\hbar^2} \sum_s \tilde{g}_{3s} \tilde{a}_{1s}^3 \int_{T_1}^{T_1+T_2} \Omega_s dt \\
&\quad \times f_s(T_1 + T_2 - t) f_s(t - T_1) f_s(t), \quad (\text{C3})
\end{aligned}$$

$$\begin{aligned}
R^{NL}(T_1, T_2) &= \frac{\alpha_0^3}{\hbar^2} \sum_s \tilde{a}_{1s}^2 \tilde{a}_{2s} \\
&\quad \times f_s(T_2) [f_s(T_1 + T_2) + f_s(T_1)]. \quad (\text{C4})
\end{aligned}$$

Here, $\tilde{a}_{2s} \equiv \tilde{a}_{1s}^2$ and the dimensionless propagator $f_s(t)$ is given by

$$f_s(t) = \frac{\Omega_s}{\zeta_s} e^{-\gamma_s t/2} \sin \zeta_s t \quad (\text{C5})$$

with $\zeta_s = \sqrt{\Omega_s^2 - \gamma_s^2/4}$.

In the mode coupling (MC) model, the response functions are expressed as

$$R^{(3)}(T_1) = \frac{\alpha_0^2}{\hbar} f_{MC}(T_1), \quad (\text{C6})$$

$$R^{(5)}(T_1, T_2) = R^{AH}(T_1, T_2) + R^{NLMC}(T_1, T_2), \quad (\text{C7})$$

where the function f_{MC} is given by

$$f_{MC}(t) = \sum_s \tilde{a}_{1s}^2 f_s(t), \quad (\text{C8})$$

and R^{NLMC} , which is equivalent to the homogeneous limit of Eq. (4.17) in Ref. 6, is given by

$$R^{NLMC}(T_1, T_2) = \frac{\alpha_0^3}{\hbar^2} f_{MC}(T_2) [f_{MC}(T_1 + T_2) + f_{MC}(T_1)]. \quad (\text{C9})$$

As mentioned in text, the third-order response function and the fifth-order signal R^{AH} are the same in the two models within the approximation. Note that $R^{(3)}$ in Eq. (C1) and Eq. (C6) as well as R^{AH} in Eq. (C2) and Eq. (C7) are the same. The spectral distribution in the two models of polarizability is then given by

$$J(\omega) = \frac{\alpha_0^2}{\hbar} \sum_s \frac{\eta_s \omega \gamma_s}{(\omega^2 - \Omega_s^2)^2 + \omega^2 \gamma_s^2}, \quad (\text{C10})$$

where the strength of the mode is defined by $\eta_s = \Omega_s \tilde{a}_{1s}^2$.

As suggested in text, the expression for $R^{NLMC}(T_1, T_2)$ given in the above is obtained easily by introducing into the Hamiltonian the source term $J_\alpha \sum_s \tilde{a}_{1s} \tilde{Q}_s$ in which the source J_α ($\alpha = 1, 2, 3$) is coupled to a collective variable $\tilde{Q} \equiv \sum_s \tilde{a}_{1s} \tilde{Q}_s$. Then derivation of R^{NLMC} becomes straightforward and, here, we only note that the propagator of this collective variable is given by

$$\sum_s a_{1s}^2 D_s^{(-+)}(t) = -i f_{MC}(t), \quad (\text{C11})$$

since the source for the collective modes can be re-expressed as $J_\alpha \sum_s a_{1s} \tilde{Q}_s$ where $a_{1s} = \tilde{a}_{1s} \sqrt{(M_s \Omega_s)/\hbar}$.

- ¹Y.-X. Yan, L.-T. Cheng, and K. A. Nelson, in *Advances in Non-linear Spectroscopy*, edited by R. J. H. Clark and R. E. Hester (Wiley, New York, 1987), p. 299; S. Ruhman, B. Kohler, A. G. Joly, and K. A. Nelson, *IEEE Quantum Electron.* **24**, 470 (1988); S. Ruhman and K. A. Nelson, *J. Chem. Phys.* **94**, 859 (1991); B. Kohler and K. A. Nelson, *J. Phys. Chem.* **96**, 6532 (1992); J. Etchepare, G. Grillon, J. P. Chambaret, G. Hamoniaux, and A. Orszag, *Opt. Commun.* **63**, 329 (1987); P. Vöhringer and N. F. Scherer, *J. Phys. Chem.* **99**, 2684 (1995); Y. J. Chang, P. Cong, and J. D. Simon, *ibid.* **99**, 7857 (1995).
- ²D. McMorrow, W. J. Lotshaw, and G. A. Kenny-Wallace, *IEEE J. Quantum Electron.* **24**, 443 (1988); C. Kalpouzos, D. McMorrow, W. J. Lotshaw, and G. A. Kenny-Wallace, *Chem. Phys. Lett.* **150**, 138 (1988); T. Hattori and T. Kobayashi, *J. Chem. Phys.* **94**, 3332 (1991); K. Wynne, C. Galli, and R. M. Hochstrasser, *Chem. Phys. Lett.* **193**, 17 (1992); Y. J. Chang and E. W. Castner, Jr., *J. Chem. Phys.* **99**, 113, 7289 (1993); S. Palese, L. Schilling, R. J. Dwayne Miller, P. R. Staver, and W. T. Lotshaw, *J. Phys. Chem.* **98**, 6308 (1994); H. P. Deuel, P. Cong, and J. D. Simon, *ibid.* **98**, 12600 (1994).
- ³M. Cho, M. Du, N. F. Scherer, G. R. Fleming, and S. Mukamel, *J. Phys. Chem.* **99**, 2410 (1993).
- ⁴D. McMorrow, N. Thantsu, J. S. Melinger, S. K. Kim and W. J. Lotshaw, *J. Phys. Chem.* **100**, 10389 (1996).
- ⁵E. Knöziger, D. Leutloff, and R. Wittenbeck, *J. Mol. Struct.* **60**, 115 (1980); G. J. Evans, *J. Chem. Soc., Faraday Trans. 2* **79**, 547 (1983); K. E. Arnold, J. Yarwood, and A. H. Price, *Mol. Phys.* **48**, 451 (1983).
- ⁶Y. Tanimura and S. Mukamel, *J. Chem. Phys.* **99**, 9496 (1993).
- ⁷K. Tominaga, Y. Naitoh, T. J. Kang, and K. Yoshihara, in *Ultrafast Phenomena IX*, edited by G. Mourou, A. H. Zewail, W. H. Knox, and P. E. Barbara (Springer, Berlin, 1994); K. Tominaga, and K. Yoshihara, *Phys. Rev. Lett.* **74**, 3061 (1995); K. Tominaga, G. P. Keogh, Y. Naitoh, and K. Yoshihara, *J. Raman Spectrosc.* **26**, 495 (1995); K. Tominaga, G. P. Keogh, and K. Yoshihara, *J. Mol. Liq.* **65/66**, 389 (1995); K. Tominaga and K. Yoshihara, *J. Chem. Phys.* **104**, 1159 (1996); K. Tominaga and K. Yoshihara, *ibid.* **104**, 4419 (1996); K. Tominaga, *Off-resonant Fifth and Seventh Order Time-Domain Nonlinear Spectroscopy on Vibrational Dephasing in Liquids*, *Advances in Multiphoton Processes and Spectroscopy*, Vol. 11 (World Scientific, Singapore, 1997, in press).
- ⁸T. Steffen and K. Duppen, *Phys. Rev. Lett.* **76**, 1224 (1996); T. Steffen and K. Duppen, in *Femtochemistry*, edited by M. Chergui (World Scientific, Singapore, 1995) p. 583; T. Steffen and K. Duppen, in *Ultrafast Phenomena*, Vol. 8, 1996 OSA Technical Digest Series (Optical Society of America, Washington D.C., 1996), p. 208; T. Steffen and K. Duppen, *J. Chem. Phys.* **106**, 3854 (1997).
- ⁹A. Tokmakoff and G. R. Fleming, *J. Chem. Phys.* **106**, 2569 (1997); A. Tokmakoff and G. R. Fleming, *Chem. Phys. Lett.* (in press).
- ¹⁰S. P. Palese, J. T. Buontempo, L. Schilling, W. T. Lotshaw, Y. Tanimura, S. Mukamel and R. J. D. Miller, *J. Phys. Chem.* **98**, 12466 (1994).
- ¹¹J. A. Leegwater and S. Mukamel, *J. Chem. Phys.* **102**, 2365 (1995); V. Khidekel and S. Mukamel, *Chem. Phys. Lett.* **240**, 304 (1995).
- ¹²A. Tokmakoff, *J. Chem. Phys.* **105**, 13 (1996).
- ¹³T. Steffen, J. T. Fourkas, and K. Duppen, *J. Chem. Phys.* **105**, 7364 (1996).
- ¹⁴M. Buchner, B. M. Ladanyi, and R. M. Stratt, *J. Chem. Phys.* **97**, 8522 (1992).
- ¹⁵H. Tanaka and I. Ohmine, *J. Chem. Phys.* **91**, 6318 (1989); I. Ohmine and H. Tanaka, *Chem. Rev.* **93**, 2545 (1993); M. Cho, G. R. Fleming, S. Saito, I. Ohmine, and R. M. Stratt, *J. Chem. Phys.* **100**, 6672 (1994); S. Saito and I. Ohmine, *ibid.* **102**, 3566 (1995); **106**, 4889 (1997).
- ¹⁶P. Moore and T. Keyes, *J. Chem. Phys.* **100**, 6709 (1994); K. Keyes, *ibid.* **104**, 9349 (1996).
- ¹⁷K. Keyes, *J. Chem. Phys.* **106**, 46 (1997).
- ¹⁸Y. J. Yan and S. Mukamel, *J. Chem. Phys.* **94**, 997 (1991).
- ¹⁹S. Mukamel, *Principles of Nonlinear Optical Spectroscopy* (Oxford University Press, New York, 1995).
- ²⁰The importance of the contribution proportional to α_2^2 to $R^{(3)}$ was studied in S. Palese, S. Mukamel, R. J. Dwayne Miller, and W. T. Lotshaw, *J. Phys. Chem.* **100**, 10380 (1996).
- ²¹In the following, we assume that the relevant values of the operator Q are confined to a small region around an equilibrium configuration. Thus we will discuss the magnitudes of terms by the expansion coefficients, such as g_3, g_4, \dots and $\alpha_0, \alpha_1, \dots$.
- ²²K. Okumura and Y. Tanimura, *Phys. Rev. E* **53**, 214 (1996).
- ²³K. Okumura and Y. Tanimura, *J. Chem. Phys.* **105**, 7294 (1996).
- ²⁴K. Okumura and Y. Tanimura, *J. Chem. Phys.* **106**, 1687 (1997).
- ²⁵K. Okumura and Y. Tanimura, *Phys. Rev. E* (submitted).
- ²⁶For a treatment of anharmonic oscillators in the level scheme instead of the coordinate scheme, see the following: J. T. Fourkas, H. Kawashima, and K. A. Nelson, *J. Chem. Phys.* **103**, 4393 (1995); J. T. Fourkas, *Theory of Vibrational Echo Phenomena in Harmonic and Weakly Anharmonic Oscillators*, Seventh International Conference on Time-Resolved Vibrational Spectroscopy, edited by W. Woodruff (1995), p. 203; J. T. Fourkas, *Laser Phys.* **5**, 656 (1995).
- ²⁷J. W. Negele and H. Orland, *Quantum Many-Particle Systems* (Addison-Wesley, New York, 1988).
- ²⁸D. Zimdars, A. Tokmakoff, S. Chen, S. R. Greenfield, M. D. Fayer, T. I. Smith, and H. A. Schwettman, *Phys. Rev. Lett.* **70**, 2718 (1993); A. Tokmakoff and M. D. Fayer, *J. Chem. Phys.* **103**, 2810 (1995).
- ²⁹W. Bosma, L. Fried, and S. Mukamel, *J. Chem. Phys.* **98**, 4413 (1993).